Confirming the trilinear form of the optical magnetoelectric effect in the polar honeycomb antiferromagnet Co2Mo3O8

Stephan Reschke, D. G. Farkas, A. Strinić, Somnath Ghara, K. Guratinder, O. Zaharko, Lilian Prodan, Vladimir Tsurkan, D. Szaller, S. Bordács, Joachim Deisenhofer, István Kézsmárki

Angaben zur Veröffentlichung / Publication details:

Reschke, Stephan, D. G. Farkas, A. Strinić, Somnath Ghara, K. Guratinder, O. Zaharko, Lilian Prodan, et al. 2022. "Confirming the trilinear form of the optical magnetoelectric effect in the polar honeycomb antiferromagnet Co2Mo3O8." *npj Quantum Materials* 7 (1): 1. https://doi.org/10.1038/s41535-021-00417-3.

npj | Quantum Materials

www.nature.com/npjquantmats

ARTICLE OPEN

Confirming the trilinear form of the optical magnetoelectric effect in the polar honeycomb antiferromagnet $Co_2Mo_3O_8$

S. Reschke[1,2], D. G. Farkas[3,4], A. Strinić[1], S. Ghara[1], K. Guratinder[5], O. Zaharko[5], L. Prodan[1], V. Tsurkan[1,6], D. Szaller[7], S. Bordács[3], J. Deisenhofer[1]✉ and I. Kézsmárki[1]

Magnetoelectric phenomena are intimately linked to relativistic effects and also require the material to break spatial inversion symmetry and time-reversal invariance. Magnetoelectric coupling can substantially affect light–matter interaction and lead to non-reciprocal light propagation. Here, we confirm on a fully experimental basis, without invoking either symmetry-based or material-specific assumptions, that the optical magnetoelectric effect in materials with non-parallel magnetization (M) and electric polarization (P) generates a trilinear term in the refractive index, $\delta n \propto k \cdot (P \times M)$, where k is the propagation vector of light. Its sharp magnetoelectric resonances in the terahertz regime, which are simultaneously electric and magnetic dipole active excitations, make $Co_2Mo_3O_8$ an ideal compound to demonstrate this fundamental relation via independent variation of M, P, and k. Remarkably, the material shows almost perfect one-way transparency in moderate magnetic fields for one of these magnetoelectric resonances.

npj Quantum Materials (2022)7:1 ; https://doi.org/10.1038/s41535-021-00417-3

INTRODUCTION

The intense research on magnetoelectric and multiferroic compounds in recent years[1–5] has revealed a plethora of novel optical phenomena specific to these materials[2,6–37]. Most of these optical effects can be rooted back to the simultaneous breaking of the time-reversal and the spatial inversion invariance in these compounds due to their coexisting magnetic and electric orderings[2,7–23,25,26,30,33,34,37,38]. Perhaps the most exotic optical effect recognized so far in magnetoelectric media is the non-reciprocal directional dichroism[6–8,10–13,15–18,20–23,25–27,29,30,32–35] when counter-propagating beams with the same initial polarization are transmitted differently through the medium. In terms of light intensity, it is manifested in the so-called directional dichroism[39,40], when the magnitude of light absorption is different for the two beams with opposite ($\pm\boldsymbol{k}$) propagation vectors. This effect is of relativistic origin and is usually considered to be weak[6–8,41,42]. However, in some compounds, the so-called one-way transparency, i.e., the maximal directional anisotropy, has been achieved in resonance with magnetoelectric excitations[17,20,22,23,29,32].

The symmetry-breaking via applied electric and magnetic fields is well-known to have profound effects on the light propagation in solids. In fact, apart from the first experimental demonstration of directional dichroism in the exciton resonances of a polar crystal in magnetic field[43], early realizations of the effect were achieved on paraelectric and paramagnetic systems subject to external electric and magnetic fields[6,42]. As pointed out by Rikken and coworkers, in materials exposed to perpendicular static electric $\boldsymbol{E}$ and magnetic $\boldsymbol{B}$ fields, the refractive index has a term proportional to $\boldsymbol{k} \cdot (\boldsymbol{E} \times \boldsymbol{B})$, hence, its magnitude is different for light propagation along $\pm\boldsymbol{k}$[6]. This polarization-independent effect was argued to be of relativistic origin, inherent to every material, since it can be traced back to the usual magnetic linear birefringence/dichroism, also called Cotton–Mouton or Voigt effect, via a Lorentz boost. The magnetic linear birefringence/dichroism, which is quadratic in B, describes the difference in the real/imaginary part of the refractive index for light polarization along and perpendicular to an externally applied magnetic field. In a frame moving with a velocity of $\boldsymbol{v} = c \cdot \boldsymbol{E} \times \boldsymbol{B}/B^2$ with respect to the original frame, there is a static electric field emerging and the optical anisotropy originally $\propto B^2$ is transformed to the directional optical anisotropy $\propto \boldsymbol{k} \cdot (\boldsymbol{E} \times \boldsymbol{B})$.

Even without considering the microscopic origin, one can generally argue on a symmetry basis that such a triple-product term can be present in the refractive index. All fundamental interactions, except for the weak interaction, obey separately the time reversal, the spatial inversion, and the charge conjugation symmetries. Therefore, if any of these three operations are simultaneously applied to the light field and the material, the measured refractive index should stay invariant. In fact, this triple-product form fulfills this condition, since either of these three operations reverses two vectors of the triple product: Time reversal switches the sign of $\boldsymbol{k}$ and $\boldsymbol{M}$, inversion reverses $\boldsymbol{k}$ and $\boldsymbol{P}$, and charge conjugation reverses $\boldsymbol{P}$ and $\boldsymbol{M}$. Concerning spatial symmetries, the triple product is an invariant scalar not only with respect to inversion but to all symmetry operations in $O(3)$, as expected for light–matter interaction.

In this first proof-of-concept, experimental studies carried out on paraelectric and or paramagnetic materials, the magnitude of the directional dichroism was found to be of the order of a few percent at most[6,42]. Since externally induced and spontaneous built-in fields are equivalent in terms of symmetry, directional dichroism of the form $\delta n \propto \boldsymbol{k} \cdot (\boldsymbol{P} \times \boldsymbol{M})$ was expected to emerge in multiferroic compounds with finite crossed polarization ($\boldsymbol{P}$)

[1]Experimental Physics V, Center for Electronic Correlations and Magnetism, Institute for Physics, Augsburg University, D-86135 Augsburg, Germany. [2]TOPTICA Photonics AG, Lochhamer Schlag 19, 82166 Gräfelfing, Germany. [3]Department of Physics, Budapest University of Technology and Economics, 1111 Budapest, Hungary. [4]Condensed Matter Research Group of the Hungarian Academy of Sciences, 1111 Budapest, Hungary. [5]Laboratory for Neutron Scattering and Imaging, Paul Scherrer Institut, CH-5232 Villigen PSI, Switzerland. [6]Institute of Applied Physics, MD-2028 Chişinău, Republic of Moldova. [7]Institute of Solid State Physics, TU Wien, 1040 Vienna, Austria.
✉email: joachim.deisenhofer@physik.uni-augsburg.de

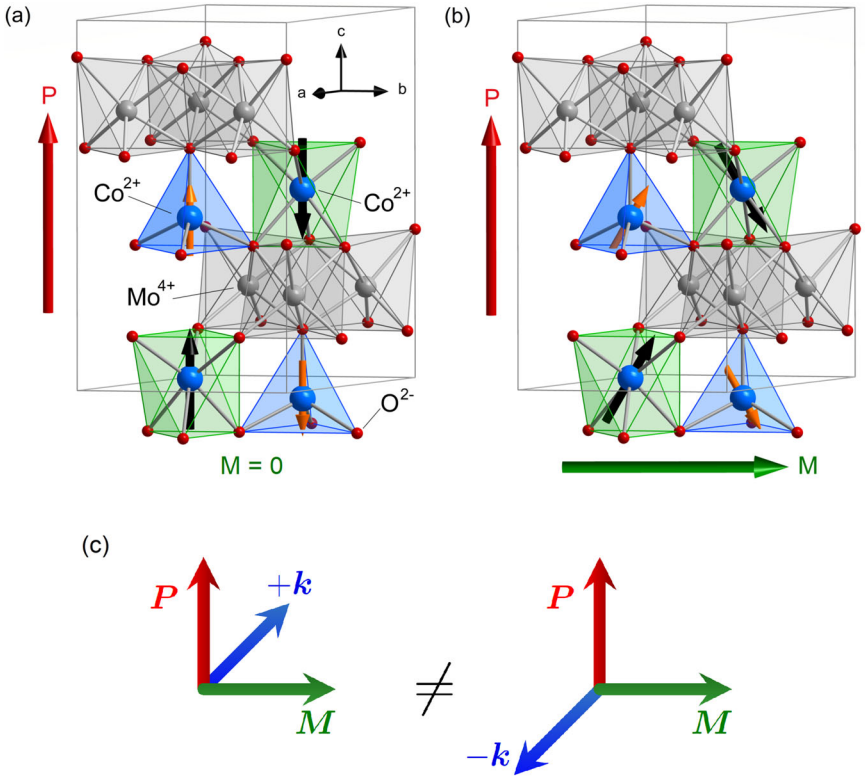

Fig. 1 Lattice structure and directional dichroism. a Crystallographic structure of $Co_2Mo_3O_8$, with ferroelectric polarization ***P*** along the *c*-axis. The magnetic Co^{2+} ions are located in both tetrahedral (blue) and octahedral (green) oxygen coordination. The antiferromagnetic spin arrangement is indicated by the arrows. **b** A magnetization *M* is induced for magnetic field $\boldsymbol{H} \perp c$ by a canting of the spins. (c) Illustration of the triple product $\boldsymbol{k} \cdot (\boldsymbol{P} \times \boldsymbol{M})$ configurations leading to directional dichroism.

and magnetization (***M***). In addition to materials with finite ***P*** and ***M***, directional optical anisotropy can produce contrast between antiferromagnetic domains[39], as demonstrated in non-centrosymmetric (antipolar) antiferromagnetic crystals, where the reversal of ***k*** is equivalent to the reversal of the antiferromagnetic Néel vector[27] or to the inversion of the quadrupole moment of the domain[33].

While the trilinear form of the directional anisotropy has not been experimentally demonstrated to the full extent in multiferroics at terahertz (THz) frequencies, the effect was found to be highly amplified by the built-in symmetry-breaking fields, in some cases leading to one-way transparency[11,20,22,23,29]. In an attempt to prove the non-reciprocal nature of light propagation, parts of the trilinear expression were verified recently in various multiferroic or magnetoelectric crystals, by showing that δn changes sign upon the flipping of ***M***[6–8,11,21,22,29,42], ***k***[23], ***M*** or ***P***[12,14,15], ***M*** or ***k***[20]. The only study, investigating the effect of the one-by-one reversal of all the three vectors and demonstrating the triple-product form of the optical magnetoelectric effect on a purely experimental basis, was carried out on the type-II multiferroic $Ba_2Mg_2Fe_{12}O_{22}$ in the microwave (GHz) regime using coplanar waveguides [26]. In our study, we demonstrate that the triple-product form of the optical magnetoelectric effect also holds when freely propagating electromagnetic waves in the THz regime are brought into interaction with a multiferroic material.

For this purpose, we chose a type-I multiferroic, more specifically the polar easy-axis antiferromagnet $Co_2Mo_3O_8$[44], as a benchmark material to systematically test the triple-product form, $\boldsymbol{k} \cdot (\boldsymbol{P} \times \boldsymbol{M})$, of the directional optical anisotropy. $Co_2Mo_3O_8$ belongs to the family of transition-metal molybdenum oxides $M_2Mo_3O_8$ (M = Mn, Fe, Co) with a hexagonal structure in the polar space group $P6_3mc$[45–51] (see Fig. 1 for the crystal structure). The Co^{2+} ions, located in both octahedrally and tetrahedrally coordinated sites, are responsible for the magnetism, as the Mo^{4+} ions from non-magnetic trimers[46,52,53]. Due to its polar crystal structure, $Co_2Mo_3O_8$ has a pyroelectric polarization ***P*** along the *c*-axis and below $T_N = 40$ K it undergoes a transition to a four-sublattice easy-axis collinear antiferromagnetic state with the Néel vector ***L*** pointing along the *c*-axis [see Fig. 1a][44,47,50,51]. Similar to other members of the $M_2Mo_3O_8$ family[53–55], the polarization of $Co_2Mo_3O_8$ is also affected by the magnetic ordering, implying a remarkable magnetoelectric coupling[44]. When the magnetic field is applied perpendicular to the *c* axis, a sizable magnetization can be induced via the canting of the spins away from the *c* axis, as sketched in Fig. 1(b). This state with perpendicular ***P*** and ***M*** is expected to exhibit directional anisotropy[12], with different refractive indices for beams traveling along the $\pm\boldsymbol{k}$ direction, as depicted in Fig. 1c.

Similar to the cases of the antiferromagnetic $Fe_2Mo_3O_8$[24], and ferrimagnetic Zn-doped $Fe_2Mo_3O_8$[25,56] and $Mn_2Mo_3O_8$[57], in the low-energy range (<16 meV) we observe two strong magnetic excitations in zero fields both in the terahertz absorption and the inelastic neutron scattering (INS) data. In contrast to the sister compounds, both of these modes in $Co_2Mo_3O_8$ are doubly degenerate and show a V-shape splitting in magnetic fields applied along the *c*-axis, as expected for a four-sublattice easy-axis collinear antiferromagnet. When $Co_2Mo_3O_8$ is magnetized perpendicular to the *c*-axis, i.e., perpendicular to its pyroelectric polarization, these modes exhibit strong directional dichroism for light beams propagating perpendicular to both ***P*** and ***M***. We systematically demonstrate via the sequential change of ***k***, ***P***, and ***M*** that the observed directional dichroism corresponds to a trilinear term in the refractive index, $\delta n \propto \boldsymbol{k} \cdot (\boldsymbol{P} \times \boldsymbol{M})$. Besides these dominant features, additional weaker excitations are resolved in the antiferromagnetic state by THz transmission spectroscopy.

RESULTS AND DISCUSSION

Dispersion of the magnetic excitations

According to linear spin-wave theory, in a simple collinear antiferromagnet, the number of magnon modes at each wavevector is expected to be equal to the number of magnetic sublattices. Given that $Co_2Mo_3O_8$ realizes a four sublattice collinear antiferromagnetic order below T_N, four modes are expected, which form two doublets in zero field.

For the first time in the $M_2Mo_3O_8$ crystal family (where M stands for a metal ion), the magnon dispersion of $Co_2Mo_3O_8$ was measured in a zero magnetic field. The results along the $(h, 0, 0)$ and $(-1, 0, l)$ directions, obtained by energy scans in INS, are shown in Fig. 2a, b, respectively. As expected for a four-sublattice antiferromagnetic order, below T_N in zero field two intense modes are observed for both directions, which are located around 5 and 10.5 meV in the zone center. Along the $(h, 0, 0)$-line, both branches show a clear dispersion, while no dispersion can be resolved along the $(-1, 0, l)$-line. This indicates that the antiferromagnetic exchange between Co sites in the same honeycomb layer is the dominant magnetic interaction and interlayer exchange coupling is much weaker, as also found for $Mn_2Mo_3O_8$[57].

Figure 2 provides a direct comparison between the energy of the two magnon modes resolved by INS and the energy of the modes observed in the THz absorption spectra in the zone center for light polarization $\boldsymbol{E}^{\omega}\|c$ & $\boldsymbol{H}^{\omega}\|a$. The two modes found in the inelastic neutron data show up as the strongest features in the absorption spectrum, centered at $41\,\mathrm{cm}^{-1} \approx 5.1$ meV and $85\,\mathrm{cm}^{-1} \approx 10.6$ meV. However, a closer inspection of the THz spectra reveals additional weaker modes at 71 and $119\,\mathrm{cm}^{-1}$. Please note that the considerably lower energy resolution of the neutron scattering experiment does not allow making a statement on the sharp and weak mode at $71\,\mathrm{cm}^{-1}$, while the energy range of the other mode is uncovered by the current neutron study. Concerning the origin of the additional modes observed in the THz measurements, these may be identified either with low-lying

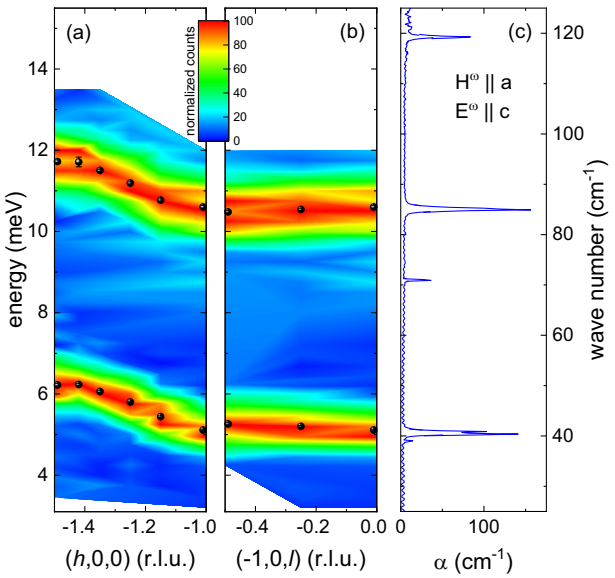

Fig. 2 Comparison of magnon dispersion and THz spectra. a, b Dispersion of magnon modes along the $(h, 0, 0)/(-1, 0, l)$ direction, as determined from inelastic neutron scattering. Symbols indicate the mode energies for the particular energy scans. The color coding represents the normalized neutron count. **c** Absorption spectrum with absorption coefficient α measured at 2 K in zero magnetic field for light polarization $\boldsymbol{E}^{\omega}\|c$ & $\boldsymbol{H}^{\omega}\|a$. For direct comparison of the zone-center energies, as obtained by the two techniques, all frames share a common vertical scale, with energy/frequency units displayed on the left/right axis.

transitions of primarily orbital character or with spin-stretching modes present in anisotropic spin systems with $S > 1/2$[58].

Field evolution and selection rules of the modes

The magnetic field dependence of the absorption spectrum is shown in Fig. 3a for $\boldsymbol{E}^{\omega}\|c$ & $\boldsymbol{H}^{\omega}\|a$ in static magnetic fields applied parallel (red curves) and perpendicular (blue curves) to the c axis. For $\boldsymbol{H}\|c$, all modes except the one at $71\,\mathrm{cm}^{-1}$ show a V-shape splitting with an increasing magnetic field. From the shift of the mode frequencies, which is linearly proportional to the strength of the magnetic field, the effective g-factors of the different modes are determined and found to vary over an unusually wide range from 0 to 5.6 (see Table 1). In contrast, for magnetic fields applied perpendicular to the c axis, no splitting of the modes could be observed.

These observations imply that the ordered moments on all sublattices, which are co-aligned with the c-axis in zero field, acquire a canting along the magnetic field, when it is applied perpendicular to the c-axis. This leads to a uniform magnetization perpendicular to the built-in polarization, as schematically shown in Fig. 1b. In addition to measurements performed with polarization $\boldsymbol{E}^{\omega}\|c$ & $\boldsymbol{H}^{\omega}\|a$, the absorption spectra were also studied in the orthogonal polarization configuration in zero field, as shown in Fig. 3b–d. Note that besides sharp resonances the absorption spectra for $\boldsymbol{E}^{\omega}\|a$ exhibit a gradual increase toward larger wavenumbers, which we assign to the low-energy tail of the lowest-lying optical phonon. A similar feature has been reported in this frequency range for the isostructural compound $Fe_{1.86}Zn_{0.14}Mo_3O_8$ and modeled accordingly[56] using the phonon eigenfrequency of approx. $130\,\mathrm{cm}^{-1}$ observed for pure $Fe_2Mo_3O_8$[59,60]. The spectra in Fig. 3b, c reveal an additional resonance, mode E, at $80\,\mathrm{cm}^{-1}$, the strength of which is independent of the orientation of $\boldsymbol{H}^{\omega}$, but the mode is only active for $\boldsymbol{E}^{\omega}\|a$. Such an only electric-dipole active mode is not expected to exhibit directional dichroism[17]. In contrast, the directional dichroism observed for the other four resonances demonstrates unambiguously that $ME_1 - ME_4$ are magnetoelectric excitations, which are both electric- and magnetic-dipole active. The selection rules as well as the g-factors of the modes for $\boldsymbol{H}\|c$ are listed in Table 1.

Directional dichroism

According to linear-response theory, the directional dichroism at long wavelengths, i.e., in the THz or far-infrared range covered here, originates from the dynamic magnetoelectric effect[18]. In the present case, $Co_2Mo_3O_8$ has a spontaneous polarization $\boldsymbol{P}\|c$ and by applying the external magnetic field $\boldsymbol{H}\perp c$, we magnetize the material perpendicular to the c axis, $\boldsymbol{M}\|a$. This reduces the $6'm'm$ hexagonal magnetic point symmetry of the antiferromagnetic state[54] to $2'm'm$ orthorhombic symmetry and activates the time-reversal odd χ'_{ac} and χ'_{ca} components in the magnetoelectric tensor[12]. In this case, the relation $\delta n \propto \boldsymbol{k} \cdot (\boldsymbol{P} \times \boldsymbol{M})$ predicts directional dichroism for light beams propagating along and opposite to the b axis, being perpendicular to both the a and c axes. Correspondingly, the solution of the Maxwell equations yields four different values for the refractive index n, two for each of the two orthogonal linear polarization configurations[12]:

$$n_{ac}^{\pm k_b} \approx \sqrt{\epsilon'_{aa}\mu'_{cc}} \mp \chi'_{ca}, \tag{1}$$

$$n_{ca}^{\pm k_b} \approx \sqrt{\epsilon'_{cc}\mu'_{aa}} \pm \chi'_{ac}. \tag{2}$$

Here, $n_{ac}^{\pm k_b}$ and $n_{ca}^{\pm k_b}$ denote the refractive indices for light polarizations $\boldsymbol{E}^{\omega}\|a$ & $\boldsymbol{H}^{\omega}\|c$ and $\boldsymbol{E}^{\omega}\|c$ & $\boldsymbol{H}^{\omega}\|a$, respectively. States propagating in opposite directions are indicated by $\pm k_b$. ϵ'_{ij} and μ'_{ij} are time-reversal invariant components of the electric permittivity and magnetic permeability tensors, respectively. In the following, we discuss the directional dichroism in these two configurations

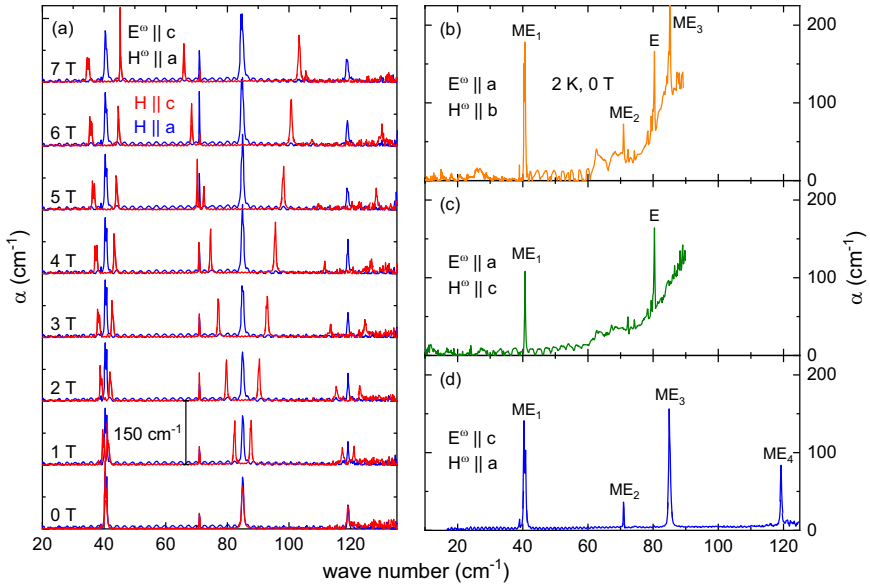

Fig. 3 THz absorption spectra in zero and finite magnetic fields. a Absorption coefficient, α, spectra measured with light polarization $\boldsymbol{E}^{\omega}\|c$ & $\boldsymbol{H}^{\omega}\|a$ at 2 K in magnetic fields $\boldsymbol{H}\|c$ (red curves) and $\boldsymbol{H}\|a$ (blue curves) up to 7 T. Spectra are shifted vertically by an offset in proportion to the magnetic field (150 cm^{-1}/T) for clarity. **b**–**d** Zero-field absorption coefficient spectra measured with the three orthogonal light polarizations at 2 K. Modes are labeled in the same way as in Table 1.

Table 1. Excitations observed in $Co_2Mo_3O_8$ below T_N.

Mode	ω_0 [cm^{-1}]	g	Polarization H_b^{ω}–E_a^{ω}	H_c^{ω}–E_a^{ω}	H_a^{ω}–E_c^{ω}	ME activity
ME_1	41	1.6	✓	✓	✓	H_c^{ω}–E_a^{ω}
ME_2	71	0.0	✓	×	✓	H_a^{ω}–E_c^{ω}
E	80	3.3	✓	✓	×	—
ME_3	85	5.6	✓	×	✓	H_a^{ω}–E_c^{ω}
ME_4	119	3.7	✓	n.r.	✓	H_a^{ω}–E_c^{ω}

For each mode, we list the resonance frequency ω_0 and the effective g-factor for $\boldsymbol{H}\|c$, and specify in which polarization configurations the mode is observed/silent (✓/×) in zero field. Mode ME_4 at 119 cm^{-1} was not resolved (n.r.) in one polarization configuration because of a low-lying phonon mode with high absorption in the corresponding spectral range. The last column refers to the polarization configuration, where the directional dichroism is observed.

and sequentially reverse $\boldsymbol{k}$, $\boldsymbol{P}$, and $\boldsymbol{M}$, in order to prove the trilinear form of the optical magnetoelectric effect.

Figure 4a, b shows the absorption spectra at 2 K for the two polarization configurations measured in positive (red) and negative (blue) magnetic fields $\boldsymbol{H}\|a$. For the polarization $\boldsymbol{E}^{\omega}\|a$ & $\boldsymbol{H}^{\omega}\|c$, directional dichroism shows up for the ME_1 mode at 41 cm^{-1} at finite magnetic fields. The absorption strength varies linearly with the magnetic field (or the induced transverse magnetization), i.e., it is enhanced and reduced for positive and negative magnetic fields, respectively. Notably, in −7 T the absorption of this resonance is almost fully suppressed and one-way transparency is nearly achieved, as will be directly evidenced in the following by the reversal of the propagation direction.

For the orthogonal light polarization $\boldsymbol{E}^{\omega}\|c$ & $\boldsymbol{H}^{\omega}\|a$ the absorption strength of the ME_1 mode at 41 cm^{-1} is independent of the magnetic field, while for the modes ME_2, ME_3, ME_4 at 71, 85, and 119 cm^{-1}, respectively, the absorption coefficient shows a field dependence. However, in this case, it is reduced for positive

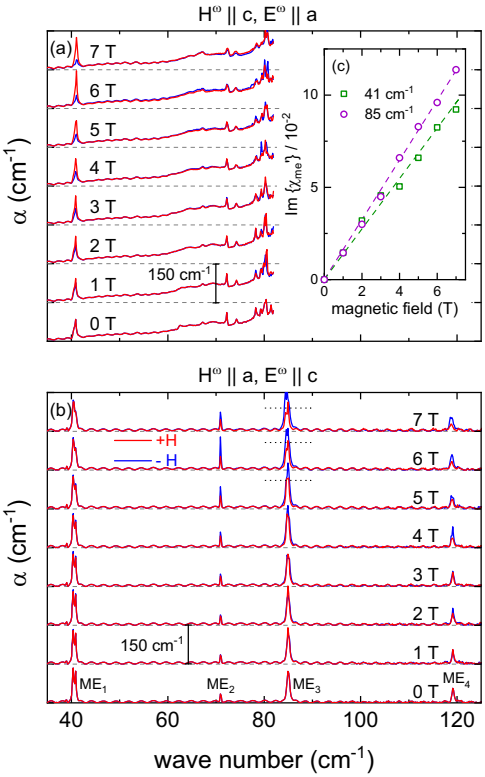

Fig. 4 Directional dichroism via inversion of the magnetic field. Magnetic field dependence ($\boldsymbol{H}\|a$) of the absorption spectra at 2 K for polarization **a** $\boldsymbol{H}^{\omega}\|c$ & $\boldsymbol{E}^{\omega}\|a$ and **b** $\boldsymbol{H}^{\omega}\|a$ & $\boldsymbol{E}^{\omega}\|c$. Red and blue curves correspond to positive and negative magnetic fields, respectively. **c** Magnetic field dependence of the peak value of the imaginary part of χ'_{me} for the modes ME_1 and ME_3. Note that the maximum absorption peak for the latter is not fully resolved due to its high absorption strength, as indicated by dashed lines.

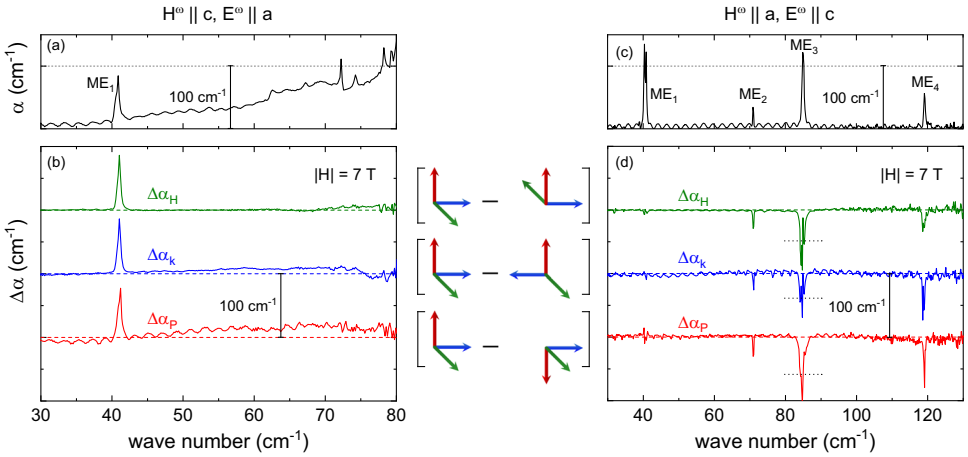

Fig. 5 Absorption difference spectra due to directional dichroism. a Absorption spectra measured at 2 K and zero magnetic field for polarization $\boldsymbol{H}^{\omega}\|c$ & $\boldsymbol{E}^{\omega}\|a$. **b** Absorption difference spectra $\Delta\alpha_H$, $\Delta\alpha_k$, and $\Delta\alpha_P$ for the same polarization in $|H| = 7$ T for $\boldsymbol{H}\|a$. For clarity, curves are shifted vertically by constant offsets of 100 cm^{-1}. **c**, **d** Corresponding set of data for the perpendicular polarization direction $\boldsymbol{H}^{\omega}\|a$ & $\boldsymbol{E}^{\omega}\|c$. Dashed lines across the ME_3 mode at 85 cm^{-1} indicate that due to the high absorption strength the peak maximum could not be fully resolved. The arrows represent the orientations of $\boldsymbol{k}$, $\boldsymbol{P}$, and $\boldsymbol{M}$, following the color scheme of Fig. 1c.

and enhanced for negative fields. According to Eqs. (1) and (2), this leads to the same sign of χ'_{ca} and χ'_{ac}, generating the directional dichroism in the first and the second polarization configuration, respectively.

The spectra of the magnetoelectric coefficients can be calculated from the absorption difference between oppositely magnetized states of the material according to

$$\mathrm{Im}\{\chi'(\omega)\} = \frac{c}{4\omega}\Delta\alpha_M(\omega) = \frac{c}{4\omega}\{\alpha(\omega)[+\boldsymbol{k},+\boldsymbol{P},+\boldsymbol{M}] - \alpha(\omega)[+\boldsymbol{k},+\boldsymbol{P},-\boldsymbol{M}]\}. \quad (3)$$

The imaginary part of the dimensionless magnetoelectric coefficient spectrum χ'_{ca} has a well-resolved maximum at 41 cm^{-1}, which follows a linear field dependence, as shown in Fig. 4c. For the mode at 85 cm^{-1}, the absorption peak is not properly resolved due to the high absorption, thus the foot of this absorption peak was fitted by a Lorentzian for both field directions to estimate the value of χ'_{ac} at the resonance. The corresponding values of $\mathrm{Im}\{\chi'_{ac}\}$, also plotted in Fig. 4c, follow a linear field dependence similar to $\mathrm{Im}\{\chi'_{ca}\}$.

In order to prove that the term in the refractive index is also an odd function of $\boldsymbol{P}$ as well as $\boldsymbol{k}$, we study the absorption coefficient upon the reversal of either the polarization of the material or the light propagation direction. Since the material is pyroelectric, the polarization $\boldsymbol{P}$ cannot be reversed by applying an electric field, instead of by rotating the sample by 180° about the a-axis. The reversal of the propagation direction $\boldsymbol{k}$ is conveniently done, without any rearrangement of the rest of the optical path, by exchanging THz emitter and receiver in our fiber-coupled Teraflash device. Both of these operations can be performed independently of each other and of the sign change of the magnetic field.

The three absorption difference spectra $\Delta\alpha_M(\omega)$, $\Delta\alpha_P(\omega)$ and $\Delta\alpha_k(\omega)$ are calculated based on experiments carried out at 2 K with $\boldsymbol{H}\|a$ and $\mu_0|H| = 7$ T according to

$$\Delta\alpha_M(\omega) = \alpha(\omega)[+\boldsymbol{k},+\boldsymbol{P},+\boldsymbol{M}] - \alpha(\omega)[+\boldsymbol{k},+\boldsymbol{P},-\boldsymbol{M}], \quad (4)$$

$$\Delta\alpha_P(\omega) = \alpha(\omega)[+\boldsymbol{k},+\boldsymbol{P},+\boldsymbol{M}] - \alpha(\omega)[+\boldsymbol{k},-\boldsymbol{P},+\boldsymbol{M}], \quad (5)$$

$$\Delta\alpha_k(\omega) = \alpha(\omega)[+\boldsymbol{k},+\boldsymbol{P},+\boldsymbol{M}] - \alpha(\omega)[-\boldsymbol{k},+\boldsymbol{P},+\boldsymbol{M}]. \quad (6)$$

The corresponding spectra are shown in Fig. 5 for both polarization directions. The inset in the middle of the figure is a graphical illustration of how the three absorption differences are calculated according to the three equations above.

The three absorption difference spectra $\Delta\alpha_M$, $\Delta\alpha_P$, and $\Delta\alpha_k$ for all magnetoelectric modes show very good agreement and nicely coincide for modes ME_1 and ME_3, as expected if the refractive index contains a term $\delta n \propto \boldsymbol{k}\cdot(\boldsymbol{P}\times\boldsymbol{M})$. The observation that the agreement for mode ME_4 is not as good as for the other modes is likely explained by the vicinity of this mode to the high-frequency cutoff of our experimental setup, which leads to a lower signal-to-noise ratio and stability in that spectral range and, thus, a poorer reproducibility in the $\pm\boldsymbol{k}$ or $\pm\boldsymbol{P}$ experiments. Remarkably, for the polarization $\boldsymbol{E}^{\omega}\|a$ & $\boldsymbol{H}^{\omega}\|c$ the absorption difference in 7 T, displayed in Fig. 5b, is larger than the total absorption in zero field [Fig. 5a] for the ME_1 mode. In the $\boldsymbol{E}^{\omega}\|c$ & $\boldsymbol{H}^{\omega}\|a$ polarization configuration, the absorption difference in 7 T, plotted in Fig. 5d, for ME_2, ME_3, and ME_4 is close to or larger than the absorption in zero field [Fig. 5c]. Specific to ME_3, the absorption peak is too strong to be fully resolved in 7 T. By fitting the flanks of $\Delta\alpha$ spectra with a Lorentzian line (not shown here) yields the maximum absorption difference $\Delta\alpha \approx 200$ cm^{-1}, a value nearly twice as large as the absorption in zero field. We want to point out that out of the four magnetoelectric resonances one-way transparency[17] is most closely realized for mode ME_1, where the resonant absorption is almost completely suppressed in -7 T, as seen in Fig. 4a.

To summarize, by independent reversal of magnetization, polarization, and light propagation, all three possibilities of realizing directional dichroism have been demonstrated for spin-wave excitations in the THz or far-infrared spectral range. Our THz spectroscopy results, performed on the collinear antiferromagnet $Co_2Mo_3O_8$ with orthogonal magnetization and polarization, directly confirm the trilinear-product form of the optical magnetoelectric effect $\boldsymbol{k}\cdot(\boldsymbol{P}\times\boldsymbol{M})$. So far this product form has been confirmed on a purely experimental basis only for the propagation of GHz frequency waveguide modes in $Ba_2Mg_2Fe_{12}O_{22}$[26]. This compound is type-II multiferroic with a transverse conical structure, which has a long (~20 nm) periodicity[61] and soft collective spin excitations in the sub-20 GHz range. In contrast, $Co_2Mo_3O_8$ is a type-I multiferroic with a simple collinear Néel order and considerably harder antiferromagnetic magnons located in the THz regime. The distinct static and dynamic properties of these two compounds and the different spectral ranges investigated in the two studies imply that non-reciprocal light propagation in multiferroics with

orthogonal ***P*** and ***M*** is generally governed by the optical magnetoelectric effect of trilinear form. The simple optical scheme and the well-defined geometry used in the present study, i.e., freely propagating light waves transmitted through plane-parallel samples, allow for precise quantification of the non-reciprocal effect. On this basis, we conclude that some of the spin-wave excitations in $Co_2Mo_3O_8$ exhibit strong directional dichroism, with one of the excitations being very close to the one-way-transparency limit.

METHODS

Synthesis

Single crystals were grown by the chemical transport reaction method at temperatures between 900 and 950 °C using anhydrous $TeCl_4$ as the source of the transport agent. X-ray analysis of the crushed single crystals revealed a single phase composition with a hexagonal symmetry and space group $P6_3mc$. The room-temperature lattice constants $a = b = 5.7677(1)$ Å and $c = 9.9097(2)$ Å are close to the data reported in literature[47,51]. Single crystals were characterized by magnetometry and specific heat measurements, which confirmed the onset of long-range antiferromagnetic order at $T_N = 40$ K.

THz spectroscopy

Temperature and magnetic field-dependent time-domain THz spectroscopy measurements were performed on plane parallel *ab*- and *ac*-cut single crystals of $Co_2Mo_3O_8$ in transmission configuration. For the optical measurements, a Toptica TeraFlash time-domain THz spectrometer was used in combination with a superconducting magnet, which allows for measurements at temperatures down to 2 K and in magnetic fields up to ±7 T.

Inelastic neutron scattering

INS was measured on two co-aligned crystals with a total weight of 800 mg using the thermal neutron triple-axis spectrometer EIGER at the SINQ, Paul Scherrer Institut, Switzerland. The use of a double-focusing PG (002) monochromator and analyzer gave the energy resolution 0.7 meV at the elastic line. The final wave vector $k_f = 2.66$ Å^{-1} was filtered by a PG filter. The sample was mounted in a ILL cryostat with the *ac*-plane horizontal, which gave access to excitations along the principal directions $(h, 0, 0)$ and $(-1, 0, l)$.

DATA AVAILABILITY

The data that support the findings of this study are available from the corresponding author upon reasonable request.

Received: 2 August 2021; Accepted: 10 December 2021;
Published online: 10 January 2022

REFERENCES

1. Tokura, Y., Kawasaki, M. & Nagaosa, N. Emergent functions of quantum materials. *Nat. Phys.* **13**, 1056–1068 (2017).
2. Tokura, Y. & Nagaosa, N. Nonreciprocal responses from non-centrosymmetric quantum materials. *Nat. Commun.* **9**, 3740 (2018).
3. Kocsis, V. et al. Magnetization-polarization cross-control near room temperature in hexaferrite single crystals. *Nat. Commun.* **10**, 1247 (2019).
4. Weymann, L. et al. Unusual magnetoelectric effect in paramagnetic rare-earth langasite. *npj Quantum Mater.* **5**, 61 (2020).
5. Cano, A., Meier, D., Trassin, M. (eds.). Multiferroics: fundamentals and applications. *De Gruyter* https://doi.org/10.1515/9783110582130 (2021).
6. Rikken, G. L. J. A., Strohm, C. & Wyder, P. Observation of magnetoelectric directional anisotropy. *Phys. Rev. Lett.* **89**, 133005 (2002).
7. Jung, J. H. et al. Optical magnetoelectric effect in the polar $GaFeO_3$ ferrimagnet. *Phys. Rev. Lett.* **93**, 037403 (2004).
8. Kubota, M. et al. X-ray directional dichroism of a polar ferrimagnet. *Phys. Rev. Lett.* **92**, 137401 (2004).
9. Pimenov, A. et al. Possible evidence for electromagnons in multiferroic manganites. *Nat. Phys.* **2**, 97–100 (2006).
10. Saito, M., Ishikawa, K., Taniguchi, K. & Arima, T. Magnetic control of crystal chirality and the existence of a large magneto-optical dichroism effect in CuB_2O_4. *Phys. Rev. Lett.* **101**, 117402 (2008).
11. Saito, M., Taniguchi, K. & Arima, T. Gigantic optical magnetoelectric effect in CuB_2O_4. *J. Phys. Soc. Jpn.* **77**, 013705 (2008).
12. Kézsmárki, I. et al. Enhanced directional dichroism of terahertz light in resonance with magnetic excitations of the multiferroic $Ba_2CoGe_2O_7$ oxide compound. *Phys. Rev. Lett.* **106**, 057403 (2011).
13. Bordács, S. et al. Chirality of matter shows up via spin excitations. *Nat. Phys.* **8**, 734–738 (2012).
14. Takahashi, Y., Shimano, R., Kaneko, Y., Murakawa, H. & Tokura, Y. Magnetoelectric resonance with electromagnons in a perovskite helimagnet. *Nat. Phys.* **8**, 121–125 (2012).
15. Takahashi, Y., Yamasaki, Y. & Tokura, Y. Terahertz magnetoelectric resonance enhanced by mutual coupling of electromagnons. *Phys. Rev. Lett.* **111**, 037204 (2013).
16. Szaller, D., Bordács, S. & Kézsmárki, I. Symmetry conditions for nonreciprocal light propagation in magnetic crystals. *Phys. Rev. B* **87**, 014421 (2013).
17. Kézsmárki, I. et al. One-way transparency of four-coloured spin-wave excitations in multiferroic materials. *Nat. Commun.* **5**, 3203 (2014).
18. Szaller, D. et al. Effect of spin excitations with simultaneous magnetic- and electric-dipole character on the static magnetoelectric properties of multiferroic materials. *Phys. Rev. B* **89**, 184419 (2014).
19. Kuzmenko, A. M. et al. Giant gigahertz optical activity in multiferroic ferroborate. *Phys. Rev. B* **89**, 174407 (2014).
20. Kuzmenko, A. M. et al. Large directional optical anisotropy in multiferroic ferroborate. *Phys. Rev. B* **92**, 184409 (2015).
21. Kézsmárki, I. et al. Optical diode effect at spin-wave excitations of the room-temperature multiferroic $BiFeO_3$. *Phys. Rev. Lett.* **115**, 127203 (2015).
22. Bordács, S. et al. Unidirectional terahertz light absorption in the pyroelectric ferrimagnet $CaBaCo_4O_7$. *Phys. Rev. B* **92**, 214441 (2015).
23. Toyoda, S. et al. One-way transparency of light in multiferroic CuB_2O_4. *Phys. Rev. Lett.* **115**, 267207 (2015).
24. Kurumaji, T. et al. Electromagnon resonance in a collinear spin state of the polar antiferromagnet $Fe_2Mo_3O_8$. *Phys. Rev. B* **95**, 020405 (2017).
25. Kurumaji, T. et al. Optical magnetoelectric resonance in a polar magnet $(Fe, Zn)_2Mo_3O_8$ with axion-type coupling. *Phys. Rev. Lett.* **119**, 077206 (2017).
26. Iguchi, Y., Nii, Y. & Onose, Y. Magnetoelectrical control of nonreciprocal microwave response in a multiferroic helimagnet. *Nat. Commun.* **8**, 15252 (2017).
27. Kocsis, V. et al. Identification of antiferromagnetic domains via the optical magnetoelectric effect. *Phys. Rev. Lett.* **121**, 057601 (2018).
28. Kuzmenko, A. M. et al. Switching of magnons by electric and magnetic fields in multiferroic borates. *Phys. Rev. Lett.* **120**, 027203 (2018).
29. Yu, S. et al. High-temperature terahertz optical diode effect without magnetic order in polar $FeZnMo_3O_8$. *Phys. Rev. Lett.* **120**, 037601 (2018).
30. Szaller, D., Shuvaev, A., Mukhin, A. A., Kuzmenko, A. M. & Pimenov, A. Controlling of light with electromagnons. *Phys. Sci. Rev.* **5**, 0055 (2019).
31. Kuzmenko, A. M. et al. Sign change of polarization rotation under time or space inversion in magnetoelectric $YbAl_3(BO_3)_4$. *Phys. Rev. B* **99**, 224417 (2019).
32. Viirok, J. et al. Directional dichroism in the paramagnetic state of multiferroics: A case study of infrared light absorption in $Sr_2CoSi_2O_7$ at high temperatures. *Phys. Rev. B* **99**, 014410 (2019).
33. Kimura, K., Katsuyoshi, T., Sawada, Y., Kimura, S. & Kimura, T. Imaging switchable magnetoelectric quadrupole domains via nonreciprocal linear dichroism. *Commun. Mater.* **1**, 39 (2020).
34. Yokosuk, M. O. et al. Nonreciprocal directional dichroism of a chiral magnet in the visible range. *npj Quantum Mater.* **5**, 20 (2020).
35. Vít, J. et al. Terahertz detection of in-situ switching between antiferromagnetic domains in the multiferroic $Ba_2CoGe_2O_7$. *Phys. Rev. Lett.* **127**, 157201 (2021).
36. Weymann, L., Shuvaev, A., Pimenov, A., Mukhin, A. A. & Szaller, D. Magnetic equivalent of electric superradiance in yttrium-iron-garnet films. *Commun. Phys.* **4**, 97 (2021).
37. Toyoda, S., Fiebig, M., Arima, T.-h., Tokura, Y. & Ogawa, N. Nonreciprocal second harmonic generation in a magnetoelectric material. *Sci. Adv.* **7**, eabe2793 (2021).
38. Cheong, S.-W., Mostovoy, M., Talbayev, D., Kiryukhin, V. & Saxena, A. Broken symmetries, non-reciprocity, and multiferroicity. *npj Quantum Mater.* **3**, 19 (2018).
39. Brown, W. F., Shtrikman, S. & Treves, D. Possibility of visual observation of antiferromagnetic domains. *J. Appl. Phys.* **34**, 1233–1234 (1963).
40. Arima, T. Magneto-electric optics in non-centrosymmetric ferromagnets. *J. Phys.* **20**, 434211 (2008).
41. Krichevtsov, B. B., Pavlov, V. V., Pisarev, R. V. & Gridnev, V. N. Magnetoelectric spectroscopy of electronic transitions in antiferromagnetic cr_2o_3. *Phys. Rev. Lett.* **76**, 4628–4631 (1996).
42. Shimada, Y., Matsubara, M., Kaneko, Y., He, J.-P. & Tokura, Y. Magnetoelectric emission in a magnetic ferroelectric Er-doped (Ba, Sr)TiO_3. *Appl. Phys. Lett.* **89**, 101112 (2006).

43. Hopfield, J. J. & Thomas, D. G. Photon momentum effects in the magneto-optics of excitons. *Phys. Rev. Lett.* **4**, 357–359 (1960).
44. Tang, Y. S. et al. Collinear magnetic structure and multiferroicity in the polar magnet $Co_2Mo_3O_8$. *Phys. Rev. B* **100**, 134112 (2019).
45. McCarroll, W. H., Katz, L. & Ward, R. Some ternary oxides of tetravalent molybdenum. *J. Am. Chem. Soc.* **79**, 5410–5414 (1957).
46. Varret, F., Czeskleba, H., Hartmann-Boutron, F. & Imbert, P. Étude par effet Mössbauer de l'ion Fe^{2+} en symétrie trigonale dans les composés du type $(Fe, M)_2Mo_3O_8$ (M = Mg, Zn, Mn, Co, Ni) et propriétés magnétiques de $(Fe, Zn)_2Mo_3O_8$. *J. Phys.* **33**, 549–564 (1972).
47. Bertrand, D. & Kerner-Czeskleba, H. Étude structurale et magnétique de molybdates d'éléments de transition. *J. Phys.* **36**, 379–390 (1975).
48. Le Page, Y. & Strobel, P. Structure of iron(II) molybdenum(IV) oxide $Fe_2Mo_3O_8$. *Acta Cryst. B* **38**, 1265–1267 (1982).
49. Strobel, P., Le Page, Y. & McAlister, S. P. Growth and physical properties of single crystals of $Fe^{II}_2Mo^{II}_2O_8$. *J. Solid State Chem.* **42**, 242–250 (1982).
50. McAlister, S. P. & Strobel, P. Magnetic order in $M_2Mo_3O_8$ single crystals (M = Mn, Fe, Co, Ni). *J. Magn. Magn. Mater.* **30**, 340–348 (1983).
51. Abe, H., Sato, A., Tsujii, N., Furubayashi, T. & Shimoda, M. Structural refinement of $T_2Mo_3O_8$ (T = Mg, Co, Zn and Mn) and anomalous valence of trinuclear molybdenum clusters in $Mn_2Mo_3O_8$. *J. Solid State Chem.* **183**, 379–384 (2010).
52. Cotton, F. A. Metal atom clusters in oxide systems. *Inorg. Chem.* **3**, 1217–1220 (1964).
53. Wang, Y. et al. Unveiling hidden ferrimagnetism and giant magnetoelectricity in polar magnet $Fe_2Mo_3O_8$. *Sci. Rep.* **5**, 12268 (2015).
54. Kurumaji, T., Ishiwata, S. & Tokura, Y. Doping-tunable ferrimagnetic phase with large linear magnetoelectric effect in a polar magnet $Fe_2Mo_3O_8$. *Phys. Rev. X* **5**, 031034 (2015).
55. Kurumaji, T., Ishiwata, S. & Tokura, Y. Diagonal magnetoelectric susceptibility and effect of Fe doping in the polar ferrimagnet $Mn_2Mo_3O_8$. *Phys. Rev. B* **95**, 045142 (2017).
56. Csizi, B. et al. Magnetic and vibronic terahertz excitations in Zn-doped $Fe_2Mo_3O_8$. *Phys. Rev. B* **102**, 174407 (2020).
57. Szaller, D. et al. Magnetic anisotropy and exchange paths for octahedrally and tetrahedrally coordinated Mn^{2+} ions in the honeycomb multiferroic $Mn_2Mo_3O_8$. *Phys. Rev. B* **102**, 144410 (2020).
58. Penc, K. et al. Spin-stretching modes in anisotropic magnets: Spin-wave excitations in the multiferroic $Ba_2CoGe_2O_7$. *Phys. Rev. Lett.* **108**, 257203 (2012).
59. Reschke, S. et al. Structure, phonons, and orbital degrees of freedom in $Fe_2Mo_3O_8$. *Phys. Rev. B* **102**, 094307 (2020).
60. Stanislavchuk, T. N. et al. Spectroscopic and first principle DFT+eDMFT study of complex structural, electronic, and vibrational properties of $M_2Mo_3O_8$ (M = Fe, Mn) polar magnets. *Phys. Rev. B* **102**, 115139 (2020).
61. Ishiwata, S. et al. Neutron diffraction studies on the multiferroic conical magnet $Ba_2Mg_2Fe_{12}O_{22}$. *Phys. Rev. B* **81**, 174418 (2010).

ACKNOWLEDGEMENTS

J.D. acknowledges stimulating discussions with Prof. Jorge Stephany. This research was partly funded by Deutsche Forschungsgemeinschaft DFG via the Transregional Collaborative Research Center TRR 80 "From Electronic correlations to the functionality" (Augsburg, Munich, Stuttgart). This work was partly performed at SINQ, Paul Scherrer Institute, Villigen, Switzerland. We acknowledge U. Stuhr for technical support during the Eiger experiment. The support via the project ANCD 20.80009.5007.19 (Moldova) is also acknowledged. This research was supported by the National Research, Development, and Innovation Office - NKFIH, FK 135003, and Bolyai 00318/20/11. D.S. acknowledges the support of the Austrian Science Fund (FWF) [I 2816-N27, TAI 334-N] and that of the Austrian Agency for International Cooperation in Education and Research [WTZ HU 08/2020].

AUTHOR CONTRIBUTIONS

L.P. and V.T. synthesized and characterized the crystals; S.R., D.G.F., and A.S. performed the THz measurements; S.R., J.D., and I.K. analyzed the THz measurements; S.G., K.G., and O.Z. performed and analyzed the neutron scattering experiments. S.R., J.D., and I.K. wrote the paper with contributions from D.S. and S.B. I.K. planned the project.

FUNDING

Open Access funding enabled and organized by Projekt DEAL.

COMPETING INTERESTS

The authors declare no competing interests.

ADDITIONAL INFORMATION

Correspondence and requests for materials should be addressed to J. Deisenhofer.

Reprints and permission information is available at http://www.nature.com/reprints

Publisher's note Springer Nature remains neutral with regard to jurisdictional claims in published maps and institutional affiliations.